A kinematic study of energy barriers for crack formation in graphene tilt boundaries

Matthew Daly and Chandra Veer Singh[a)]
Department of Materials Science and Engineering, University of Toronto, 184 College Street, Suite 140, Toronto, Ontario M5S 3E4, Canada

(Received 13 February 2014; accepted 2 June 2014; published online 11 June 2014)

Recent experimental studies have observed a surprisingly wide range of strengths in polycrystalline graphene. Previous computational investigations of graphene tilt boundaries have highlighted the role of interfacial topology in determining mechanical properties. However, a rigorous characterization of deformation energy barriers is lacking, which precludes direct comparison to the available experimental data. In the current study, molecular dynamics tensile simulations are performed to quantify kinematic effects on failure initiation in a wide range of graphene tilt boundaries. Specifically, the process of crack formation is investigated to provide a conservative estimate of strength at experimental loading rates. Contrary to previous studies, significant strain rate sensitivity is observed, resulting in reductions of crack formation stresses on the order of 7% to 33%. Energy barriers for crack formation are calculated in the range of 0.58 to 2.07 eV based on an Arrhenius relation that is fit to the collected simulation data. Physically, the magnitude of energy barriers in graphene tilt boundaries is found to be linearly correlated to the pre-stress in the critical bonds. Predictions reported in the present study provide a possible explanation for the wide range of strengths experimentally observed in polycrystalline graphene and greatly improve upon current theoretical estimates. © *2014 AIP Publishing LLC*. [http://dx.doi.org/10.1063/1.4883190]

I. INTRODUCTION

With an intrinsic strength reported at above 100 GPa,[1] graphene permits access to previously uncharted areas of material-property space making it a desirable material for a number of composite applications.[2] Efforts to increase manufacturing yield have resulted in the synthesis of polycrystalline graphene,[3] with tilt boundaries separating misoriented crystallographic domains.[4] The impact of such tilt boundaries on mechanical properties is currently an area of extreme research fervor, with experimental reports of polycrystalline strength ranging from as low as 35 GPa (Ref. 5) to near pristine values of 98.5 GPa.[6] Weakening of polycrystalline graphene has previously been suggested as a result of high porosity in the graphene samples.[6] A recent atomic force microscopy investigation of high quality graphene bicrystals, however, has reported a wide strength envelope, with breaking stresses encompassing approximately the entire range observed in the previous studies (48 to 83 GPa).[7] The phenomena underpinning strength in polycrystalline graphene may, therefore, be more complicated than sample quality considerations and merits further investigation.

Tilt boundaries in graphene are known to be populated by topological defects.[4,8–10] On the atomic scale, topological defects take the form of a periodic arrangement of heptagon-pentagon disclination dipole clusters.[11–13] The density and periodicity of such defect tilings are dictated by the tessellation requirements of adjacent grains. Therefore, the tilt angle between graphene crystals determines the spacing of disclination clusters and the specific structure of the grain boundary. Relative to 3D structures, planar defects such as grain boundaries possess a greater influence on the properties of low dimensional materials. In 2D systems, a planar defect may be considered as a flaw transcending the entire thickness of a sample. It is therefore expected that the strength of polycrystalline graphene is strongly related to the interfacial configuration connecting adjacent graphene grains. Given the large range of strengths reported in existing experimental studies, a rigorous study of the strength limiting features of tilt boundaries in polycrystalline graphene is therefore required to understand the physical phenomena underscoring weakening.

Atomistic computational studies have proven extremely effective in providing mechanistic explanations for observed experimental phenomena in graphene.[14,15] The nature of weakening in polycrystalline graphene as it relates to tilt angle and topological structure has been examined in a number of theoretical investigations.[12,13,16–25] Notable athermal molecular dynamics (MD) studies have identified defect-saturated high angle boundaries as possessing both the lowest interfacial energies and the greatest strength,[12,13] supporting recent experimental characterization.[6,7] The effects of temperature on the fracture behavior of graphene tilt boundaries have also been investigated briefly in theoretical studies,[18–24] with results being qualitatively comparable to the available athermal computational investigations. Although these numerical studies have proven successful in establishing trends in mechanical properties, the vast majority of these investigations are restricted to high strain rates in a relatively narrow loading range,[17,23] which may inflate strength predictions and underestimate the impact of kinematic (i.e., temperature and

[a)]Author to whom correspondence should be addressed. Electronic mail: chandraveer.singh@utoronto.ca

TABLE I. Geometric parameters used to construct and classify the tilt boundaries studied in MD simulations.

Orientation	θ_{zz} (°)[a]	h_d (Å)	Σ
Zigzag	21.8	6.507	7
Zigzag	13.2	10.721	19
Zigzag	9.5	14.961	37
Armchair	32.2 (27.8)	8.868	13
Armchair	38.2 (21.8)	11.271	21
Armchair	42.1 (17.9)	13.693	31

[a]θ_{ac} is provided in brackets where applicable.

strain rate) effects. For instance, Yi *et al.*[23] performed uniaxial MD tensile simulations on a number of graphene tilt boundaries at strain rates ranging from 10^8 to 10^{10}/s. In this study, the authors report strain rate insensitivity with respect to strength which may be a consequence of the relatively small range of strain rates tested. Since large interfacial stresses have been observed in many of the sampled tilt boundary configurations,[13] it is likely that kinematic effects become significant at strain rates more representative of experimental conditions (e.g., at $\sim 10^0$/s in Ref. 7). From a time-scale perspective, quantification of deformation energy barriers in graphene tilt boundaries is therefore necessary to accurately capture strain rate sensitivity. To the authors' knowledge, analysis of deformation energy barriers in polycrystalline graphene is limited to a preliminary investigation of 21.7° tilted graphene bicrystals,[17] with strengths of 125 GPa predicted under quasi-static loading conditions. However, current experimental reports suggest an upper limit of approximately 98.5 GPa for polycrystalline graphene,[6] which indicates that kinematic effects are not fully captured by this computational study, rendering these strength predictions less accurate at experimental time-scales. A comprehensive characterization of the deformation energetics in graphene tilt boundaries is therefore warranted to quantify the energy barrier resisting material fracture and inform reasonable predictions of strength.

The purpose of the current work is to perform a comparative analysis of kinematic effects on mechanical failure over a wide range of graphene tilt boundaries. Recent theoretical[26–28] and experimental[29] studies have highlighted the important role crack initiation and propagation holds in the mechanical failure in graphene; however, a kinematic study of the energy barriers resisting crack formation in graphene tilt boundaries remains an open theme. Therefore, the energy barrier of the initial bond-breakage event as it relates to crack formation is selected for study. As failure in graphene is considered to be brittle in nature,[30] the crack formation stress is assumed to provide a conservative estimate of strength. Furthermore, an energy barrier analysis of crack formation may be considered critical to assessments of strength given the possibility of crack instability in graphene.[28] In order to capture the probabilistic nature of failure in polycrystalline graphene, an in-depth statistical study of critical stresses to crack formation is performed. Both lower and higher energy grain boundaries are studied in order to sample a wide range of tilt angles. Results of this study may serve to reconcile the wide strength ranges observed in experimental testing and improve the accuracy of numerical simulations.

II. COMPUTATIONAL METHODS

MD simulations are conducted using the freely available Large-scale Atomic/Molecular Massively Parallel Simulator (LAMMPS).[31] The Adaptive Intermolecular Reactive Empirical Bond Order (AIREBO) interatomic potential with a bond cutoff radius of 1.92 Å is used for all MD simulations. This cutoff radius has been validated for the AIREBO potential from independent density functional theory calculations of the stress-strain response of graphene.[13] In the current work, six different graphene tilt boundaries are investigated and their relevant structural properties are summarized in Table I. For the purposes of comparison, tilt angles reported in previous numerical[12,13,17,23] and experimental studies[6,7] are chosen for investigation. The selected tilt boundaries are characterized using coincidence site lattice theory (CSL), following the topology construction methodology and boundary classification system outlined in Ref. 32. Using the nomenclature of Grantab *et al.*[12] and Yazyev and Louie,[11] tilt boundaries may be further categorized into zigzag and armchair groups with the former constructed of (1,0) and the latter with (1,0) + (0,1) disclination dipole defects. Disclination clusters are periodically spaced over a distance h_d as required for tessellation. Figures 1(b) and 1(c) provide schematics of (1,0) and (1,0) + (0,1) disclination clusters. For the purposes of the current work, graphene tilt boundaries are referenced with respect to the CSL parameter, Σ. Zigzag oriented boundaries with a tilt angle of θ_{zz} may be described in terms of the armchair lattice angles (θ_{ac}) by the relation: $\theta_{ac} = 60 - \theta_{zz}$. Figure 2 provides the topologies of graphene tilt boundaries selected for study. As shown in the figure, athermal atomic potential energies increase in the vicinity of the disclination clusters, consistent with previous reports.[13]

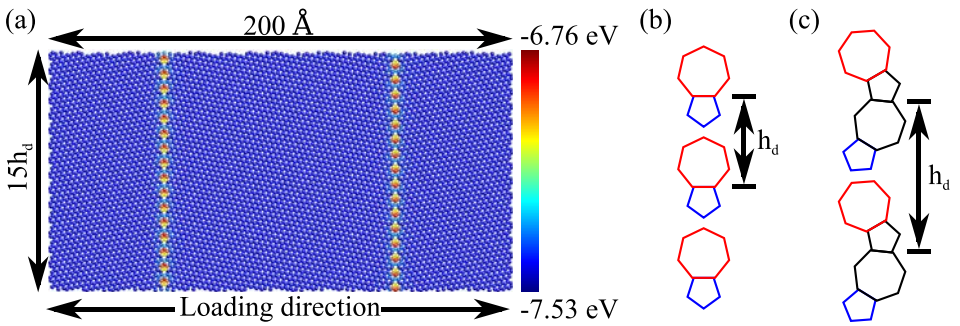

FIG. 1. (a) A representative (Σ 7) simulation supercell used in MD simulations. The loading direction is indicated in the figure and the colormap represents atomic potential energy at 0 K. Schematics of the disclination clusters which form the interfacial structure of (1,0) zigzag (b) and (1,0) + (0,1) armchair (c) graphene tilt boundaries. The distance between periodic images, h_d, is indicated in each illustration.

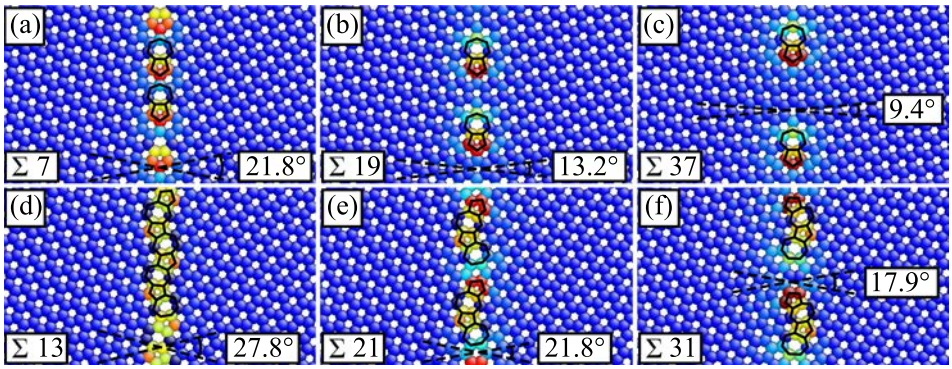

FIG. 2. Interfacial topologies of the Σ 7 (a), Σ 19 (b), Σ 37 (c) zigzag; and Σ 13 (d), Σ 21 (e), Σ 31 armchair graphene tilt boundaries. Disclination clusters are outlined in the black stroke and colormap is the same as in Figure 1.

A schematic of a typical graphene tilt boundary supercell used in MD studies is provided in Figure 1(a). Two anti-symmetric grain boundaries are constructed to enforce periodic boundary conditions and avoid unwanted stress concentrations along the supercell boundaries. Uniaxial tensile simulations are performed through application of strain-controlled deformation along the loading direction (perpendicular to the tilt boundary) indicated in Figure 1(a). This loading configuration is selected in order to provide the most conservative configuration for mechanical results. System temperature as well as Poisson effects are accommodated using the isothermal-isobaric (NPT) ensemble available in LAMMPS, wherein independent control of each axis of the pressure triad is permitted. Using this ensemble, pressures along directions orthogonal to loading are held at zero, while strain is applied incrementally in the loading direction, maintaining the uniaxial tensile condition. Based on previous studies, fracture is expected to originate along the disclination cluster line,[13,23] with each dipole acting as a potential failure nucleation site. The longitudinal dimensions of the supercell are, therefore, selected to maintain a constant number of failure initiation sites across each of the examined tilt boundaries. All tilt boundary samples possess at least 8000 atoms. Prior to tensile loading, a relaxation step is programmed to ensure a minimum system energy and to stabilize the global temperature (T). Stress is calculated as the spatial and temporal average of the combined per atom virial and thermal components and the thickness of the graphene plane is assumed to be 3.35 Å.[1] For the purposes of energy barrier calculations and strain rate sensitivity analysis, MD simulations are conducted over a large span of loading rates. Tensile studies are undertaken in the range of 5×10^6 to 10^9/s, which provides a much wider sampling of kinematic effects than previously accessed by computational studies of graphene tilt boundaries. Statistical replication of each simulation condition is achieved using the Gaussian random seed method and all simulations are conducted with a timestep of 1 fs. Visualization of atomic topologies is achieved using the AtomEye atomistic configuration viewer.[33]

III. ENERGY BARRIER ANALYSIS OF CRACK FORMATION

Energy barriers resisting failure initiation may be quantitatively sampled through measurement of global loading conditions at the instant of bond-breakage and subsequent crack formation. Since graphene is known to exhibit brittle fracture,[30] taking the crack formation event as strength limiting permits a conservative estimate for the bounds on graphene strength. In all MD simulations, crack formation is observed to occur at a disclination cluster along the tilt boundary. Figure 3 presents typical topologies in zigzag and armchair oriented tilt boundaries at the instant of crack formation (T = 300 K). Crack formation may be identified by monitoring the atomic coordination of critical bonds. In most simulations, cracks nucleate along the bond shared between the heptagon-hexagon carbon rings. In some simulations of zigzag oriented tilt boundaries, however, failure initiates from the heptagon-pentagon bond. Given the relatively small statistical scatter in each tested simulation condition, the kinematics surrounding these deformation events are expected to be quantitatively similar.

Using the thermal activation theory of Eyring,[34] the Arrhenius relationship may be used to describe the lifetime τ of a specimen as a function of loading σ and temperature T by the relation

$$\tau = \frac{\tau_o}{n_s} \exp\left(\frac{E_o - V_a \sigma}{k_b T}\right), \tag{1}$$

where τ_o is related to the vibrational frequency of crystalline oscillations, n_s is the number of sites available for thermal

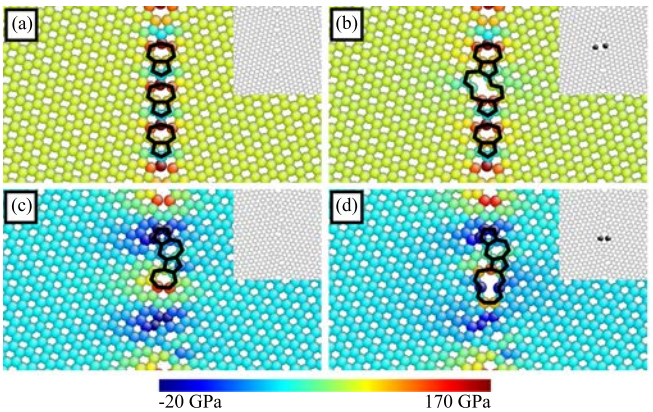

FIG. 3. Atomic topologies of Σ 7 (a), (b) and Σ 31 (c), (d) tilt boundaries immediately prior to and after crack formation at 300 K. The crack formation stress σ_c is defined as the global stress state at the instant of crack initiation. The heptagon-hexagon bond is typically found to be the critical bond in crack formation. The inset indicates atomic coordination with black and white representing coordinations of 2 and 3, respectively. The colormap represents per atom stress values along the loading direction. Disclination clusters are highlighted in black stroke.

activation, E_o is the energy barrier resisting the crack formation event, V_a is the activation volume, and k_b is the Boltzmann constant. In this formulation, E_o implicitly captures reductions in the energy barrier arising from defective structures and $V_a\sigma$ accounts for the strain energy imparted by the applied external loading. Since crack formation at the tilt boundary is the sole observed failure mechanism in all MD simulations, E_o may therefore be used to unambiguously define the energy barrier of this deformation event. This Arrhenius-based approach has been previously validated for MD studies of defective structures such as Stone-Wales defects in carbon nanotubes.[35] Following the analytical formulation provided by Zhao and Aluru,[36] Eq. (1) may be used in combination with Bailey's principle[37] to provide unique equations for the expectation time (t_c) and stress of crack formation (σ_c) as functions of $\dot{\epsilon}$ and T. In order to reconcile strain rate sensitivity with this analytical approach, an additional constitutive relation for the time dependent applied stress (i.e., $\sigma = \sigma(t)$) is required. The non-linear elastic response of graphene may be accurately represented by a logarithmic function of the form

$$\sigma(t) = a\ln(b\dot{\epsilon}t + 1). \tag{2}$$

Representative MD tensile simulations of each graphene tilt boundary are provided in Figure 4. All tilt boundaries exhibit a similar mechanical response and therefore only a singular form of Eq. (2) is required to capture the non-linear elastic behavior of each grain boundary. A least squares fit to the collected data yields $a = 93.25$ GPa and $b = 11.94$. Equation (2) can be shown to reduce to a linear relation of $\sigma \approx ab\epsilon$,[36] where $ab = 1.11$ TPa, which is approximately equal to the experimentally measured in-plane modulus of 1.02 TPa.[1] If $t = t_c$, then the crack formation stress may be defined as $\sigma_c = a\ln(b\dot{\epsilon}t_c + 1)$. As per Ref. 36, substitution of Eqs. (2) and (1) into the Bailey criterion with $t = t_c$ provides a unique expression for σ_c of the form

$$\sigma_c(\dot{\epsilon}, T) = \frac{ak_bT}{V_a a + k_bT}\left\{\frac{E_o}{k_bT} + \ln\left[\frac{b\dot{\epsilon}\tau_o}{n_s}\left(\frac{V_a a}{k_bT} + 1\right)\right]\right\}. \tag{3}$$

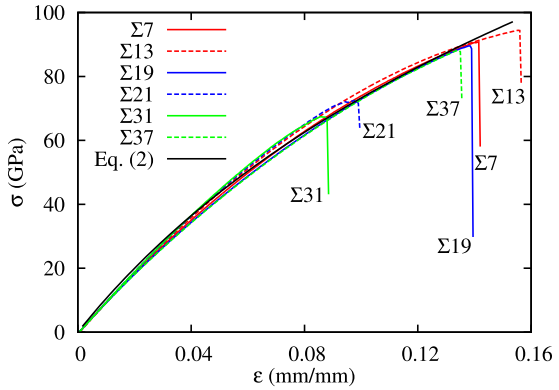

FIG. 4. Representative tensile simulations for each of the sampled tilt boundaries. Equation (2) is overlaid to show the fitted non-linear elastic response that is assumed for energy barrier calculations. MD tensile simulations are conducted here at $T = 300$ K and $\dot{\epsilon} = 10^9/s$.

The expectation time of crack formation may then be defined as

$$t_c = \tau\left(\frac{V_a a}{k_bT} + 1\right)\left(1 - \frac{1}{e^{\frac{\sigma_c}{a}}}\right). \tag{4}$$

Application of Eqs. (3) and (4) permits direct analysis of the energy barrier for crack formation. However, before the presented Arrhenius formulation is applied to the tilted graphene samples, MD simulation results should be validated against existing experimental data to provide confidence in methodology. Energy barrier analysis of pristine graphene using the experimentally determined in-plane bond dissociation energy (4.93 eV, Ref. 38) of graphite results in excellent agreement with MD data. Further details of the kinematic study of pristine graphene are provided as supplementary data.[39] The collected crack formation stresses for the graphene tilt boundary samples at $T = 300$ K are provided in Figure 5, with error bars representing 95% confidence. Each of the sampled tilt boundaries is found to exhibit some degree of strain rate sensitivity. The smallest reductions in crack formation stress are observed in the Σ 13 tilt boundary, whereas the largest reductions occur in the Σ 31 samples. These extrema of strain rate sensitivity represent reductions ranging from 7% to 33% over the approximately four orders of magnitude of sampled loading rates. These results suggest that in some cases graphene can exhibit a significant degree of strain rate sensitivity and seem to contradict previous reports declaring the insensitivity of polycrystalline graphene.[23]

The collected MD data presented in Figure 5 are fit to Eq. (3) in order to determine the energy barriers for crack formation. The fitted energies and volumes are then applied to Eq. (3) and overlaid with the collected crack formation stresses, showing excellent correlation with the MD data. In all fitting of tilt boundary data $n_s = 100$, and $\tau_o = 0.1$ ps.[40]

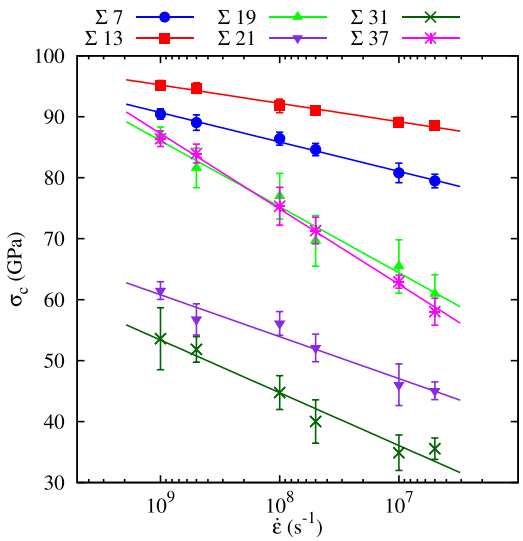

FIG. 5. Crack formation stresses σ_c of the graphene tilt boundaries as determined by MD study ($T = 300$ K). All tilt boundaries are observed to exhibit some degree of strain rate sensitivity. Equation (3) is calculated based on fitting of energy barriers and activation volumes and is plotted for each tilt boundary in the respective colored stroke, showing good agreement with MD data. Error bars represent 95% confidence ($n = 10$). In some cases, error bars fall inside the perimeter of the data markers.

Values of E_o are found to follow a similar trend to strain rate sensitivities and range from 0.58 (Σ 31) to 2.07 eV (Σ 13). Activation volumes are found to be in the range of ~1–3 Å^3, which is approximately the size of a sp^2 covalent bond. The expectation time t_c may be also evaluated using Eq. (4) from the energy barriers obtained from Eq. (3). Figure 6 provides the predicted expectation times for crack formation as a function of critical stress for each tilt boundary. Agreement with the collected MD data is good, providing confidence in the values of E_o from Eq. (3) and the validity of the presented energy barrier formulation. In order to validate the robustness of the analytical formulation with respect to temperature variations, a parallel energy barrier analysis of the Σ 7 boundary at T = 450 K is performed using E_o and V_a obtained from fitting the data in Figure 5. The results of this comparative analysis show excellent agreement across both thermal conditions and are provided in the supplementary material.[39]

In order to establish a physical rationale for trends in E_o, the pre-stress arising from tessellation mismatches in the interfacial structures of the sampled tilted boundaries is considered. Examination of relaxed interfacial topologies shows that pre-stress in bonds range from −75 to 90 GPa, in the Σ 13 and Σ 31 tilt boundaries, respectively, with the critical bond in the Σ 31 tilt boundary loaded to near the upper tensile limit of the colormap (Figure 7). These large tensile and compressive stresses in the critical crack-forming bonds are responsible for the observed differences in E_o and premature cracking in higher energy tilt boundaries. The pre-stress arising from the periodic tiling of disclination clusters in graphene tilt boundaries has been studied in depth by Wei *et al.*[13] In their study, the authors developed an analytical model to predict the normalized pre-stress acting on disclinations defects in graphene. Further information regarding disclination mechanics in graphene as well as an explanation of pre-stress normalization may be found in Ref. 41. Figure 8 provides the computed values of E_o with the disclination

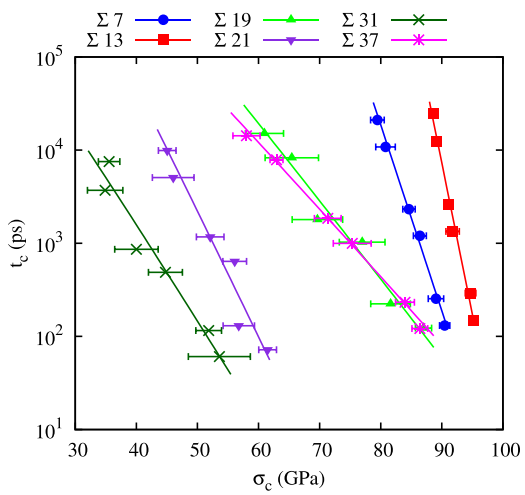

FIG. 6. Expectation times t_c for crack formation as determined by MD study (T = 300 K). Equation (4) is used to calculate expectation times with the values of energy barrier and activation volume fit from Eq. (3). The results are overlaid with the MD data for each tilt boundary in the respective colored stroke. Error bars represent 95% confidence (n = 10). In some cases, error bars fall inside the perimeter of the data markers.

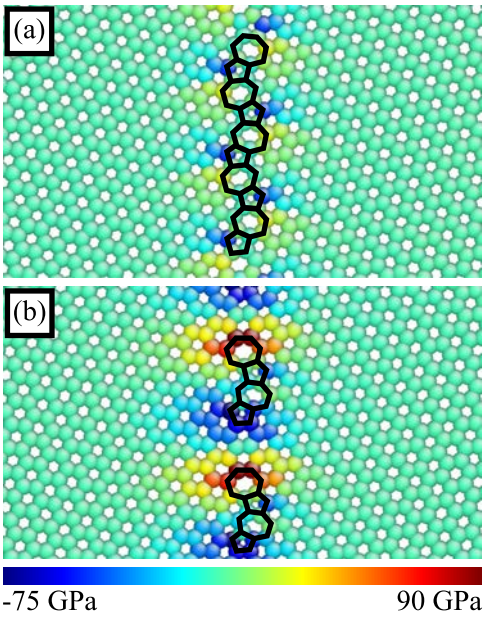

FIG. 7. Atomic topologies of the relaxed Σ 13 (a) and Σ 31 (b) tilt boundaries at T = 0 K. Pre-stress at the critical heptagon-hexagon bond reaches nearly 90 GPa in the Σ 31 structure. The colormap indicates per atom stresses along the loading direction and disclination clusters are outlined in black stroke.

normalized pre-stress (σ_p) in the critical carbon-carbon bond of each tilt boundary. Examination of the plotted data shows a remarkable linear correlation ($R^2 = 0.98$) between energy

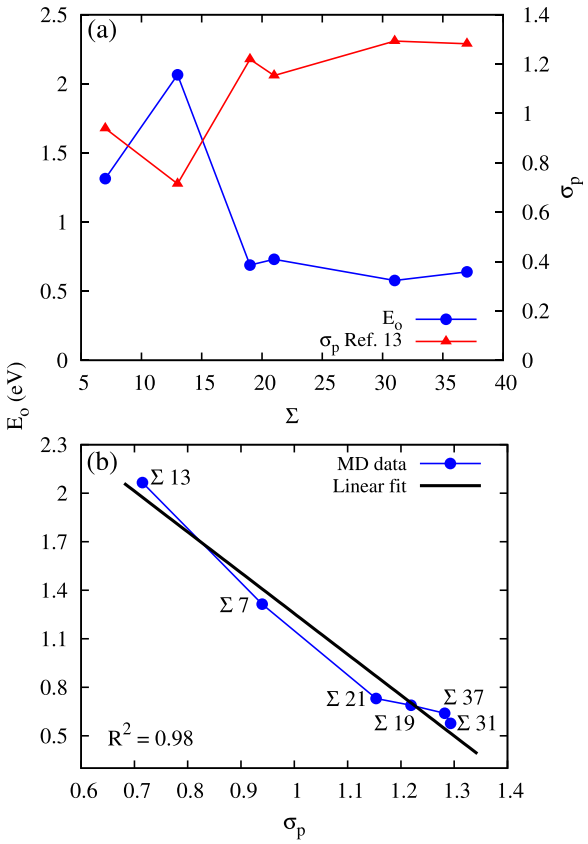

FIG. 8. (a) Energy barriers E_o are plotted alongside the normalized disclination pre-stress σ_p in the critical bond to crack formation. The pre-stress data are obtained from Ref. 13. (b) Correlation of energy barrier to bond pre-stress showing a strong linear relationship ($R^2 = 0.98$).

barriers and bond pre-stress (Figure 8(b)). Considering the physics of an Arrhenius process, a strong linear correlation is expected. This linear behavior is captured analytically in the exponent terms (i.e., $E_o - V_a\sigma$) of Eq. (1). Since external loading shows a linear relationship with E_o, pre-stress is expected to lower the energy barrier in a similar fashion. This finding shows that the bond pre-stress arising from interfacial structure has a critical role in determining the energy barrier of crack formation processes in graphene. Graphene samples with a low energy tilt boundary (e.g., Σ 13) are therefore expected to have larger crack formation stresses and thus higher strength, whereas higher energy interfacial topologies are more prone to crack formation.

Extrapolation of the collected fitting results shows that kinematic effects become more pronounced as strain rates are reduced. For example, at a strain rate of 10^9/s and T = 300 K, MD results predict crack formation strengths of 90.5 and 95.2 GPa for Σ 7 and Σ 13 tilt boundaries, respectively. However, by extending Eq. (3) to strain rates typical of experimental indentation studies (e.g., 10^0/s) crack formation stresses of 47.3 (Σ 7) and 68.1 GPa (Σ 13) are predicted. A similar calculation performed on pristine graphene loaded in the armchair direction yields a crack formation stress of 84.2 GPa. These predictions thus approximately span the range of strengths experimentally measured by Rasool *et al.*[7] (48 to 83 GPa) and fall between the bounds reported by Ruiz-Vargas *et al.*[5] (35 GPa) and Lee *et al.*[6] (98.5 GPa). Additionally, the results highlight the sensitivity of polycrystalline graphene to interfacial topology and provide a physical interpretation for the degree of weakening observed in experimental reports. Nonetheless, caution must be exercised when making direct comparisons to experiments as the precise topology of the indented tilt boundaries is unknown. Even so, the predictions presented here greatly improve on the existing theoretical estimates (e.g., 125 GPa in Ref. 17). The implication of these predictions is that the calculated energy barriers may be used to estimate a conservative range for strengths in polycrystalline graphene. The current analysis also forecasts that in some tilt boundaries (e.g., Σ 31) bond-breakage may occur spontaneously given sufficiently low loading rates and high enough temperatures. This result may be rationalized by considering the large tensile pre-stresses found in some interfacial topologies (Figure 7), but requires confirmation with experimental observations.

IV. CONCLUSIONS

The impact of kinematic effects on the crack formation stress of graphene tilt boundaries was studied via MD simulation. Results of uniaxial tensile tests indicated that, contrary to previous studies, some tilt boundaries in graphene exhibit a large degree of strain rate sensitivity. Higher energy tilt boundaries such as the Σ 31 were found to be the most sensitive to loading rate, whereas lower energy boundaries such as Σ 13 were less sensitive. Based on MD data, an Arrhenius relationship was fit to tensile results to obtain the energy barriers resisting crack formation in the examined grain boundary configurations. The resultant energy barrier values were shown to correlate strongly to the degree of pre-stress in the critical interfacial bonds for each topological structure. Although most graphene tilt boundaries showed high strength at the relatively high strain rates applied in MD simulations, kinematic effects were found to become more pronounced when loading rates approached experimental ranges, leading to a considerable drop in crack formation stresses. In comparison to existing numerical studies, the conservative predictions of strength reported in the current study were found to be much closer to experimental observations. The range of energy barriers calculated in this study highlights the importance of interfacial topology in determining the mechanical properties of graphene tilt boundaries and serves to rationalize the wide spectrum of experimentally reported strengths for polycrystalline graphene.

ACKNOWLEDGMENTS

The authors would like to acknowledge Dr. Tobin Filleter for useful discussions and the Natural Sciences and Engineering Research Council of Canada (NSERC) for providing funding for this work. Computations were performed on the GPC supercomputer at the SciNet HPC Consortium and the Briaree computing cluster under the administration of Calculquebec. SciNet is funded by: the Canada Foundation for Innovation under the auspices of Compute Canada; the Government of Ontario; Ontario Research Fund-Research Excellence; and the University of Toronto.

[1]C. Lee, X. Wei, J. W. Kysar, and J. Hone, Science **321**, 385 (2008).
[2]S. Stankovich, D. A. Dikin, G. H. B. Dommett, K. M. Kohlhaas, E. J. Zimney, E. a. Stach, R. D. Piner, S. T. Nguyen, and R. S. Ruoff, Nature **442**, 282 (2006).
[3]X. Li, W. Cai, J. An, S. Kim, J. Nah, D. Yang, R. Piner, A. Velamakanni, I. Jung, E. Tutuc, S. K. Banerjee, L. Colombo, and R. S. Ruoff, Science **324**, 1312 (2009).
[4]K. Kim, Z. Lee, W. Regan, C. Kisielowski, M. F. Crommie, and A. Zettl, ACS Nano **5**, 2142 (2011).
[5]C. S. Ruiz-Vargas, H. L. Zhuang, P. Y. Huang, A. M. van der Zande, S. Garg, P. L. McEuen, D. A. Muller, R. G. Hennig, and J. Park, Nano Lett. **11**, 2259 (2011).
[6]G.-H. Lee, R. C. Cooper, S. J. An, S. Lee, A. van der Zande, N. Petrone, A. G. Hammerberg, C. Lee, B. Crawford, W. Oliver, J. W. Kysar, and J. Hone, Science **340**, 1073 (2013).
[7]H. I. Rasool, C. Ophus, W. S. Klug, A. Zettl, and J. K. Gimzewski, Nature Commun. **4**, 2811 (2013).
[8]J. An, E. Voelkl, J. J. Suk, X. Li, C. W. C. Magnuson, L. Fu, P. Tiemeijer, M. Bischoff, B. Freitag, E. Popova, and R. S. Ruoff, ACS Nano **5**, 2433 (2011).
[9]P. Y. Huang, C. S. Ruiz-Vargas, A. M. van der Zande, W. S. Whitney, M. P. Levendorf, J. W. Kevek, S. Garg, J. S. Alden, C. J. Hustedt, Y. Zhu, J. Park, P. L. McEuen, and D. A. Muller, Nature **469**, 389 (2011).
[10]B. I. Yakobson and F. Ding, ACS Nano **5**, 1569 (2011).
[11]O. V. Yazyev and S. G. Louie, Phys. Rev. B **81**, 195420 (2010).
[12]R. Grantab, V. V. Shenoy, and R. S. Ruoff, Science **330**, 946 (2010).
[13]Y. Wei, J. Wu, H. Yin, X. Shi, R. Yang, and M. Dresselhaus, Nature Mater. **11**, 759 (2012).
[14]M. Neek-Amal and F. M. Peeters, Phys. Rev. B **82**, 085432 (2010).
[15]M. Neek-Amal and F. M. Peeters, Appl. Phys. Lett. **97**, 153118 (2010).
[16]A. Cao and J. Qu, Appl. Phys. Lett. **102**, 071902 (2013).
[17]A. Cao and J. Qu, J. Appl. Phys. **112**, 043519 (2012).
[18]A. Cao and Y. Yuan, Appl. Phys. Lett. **100**, 211912 (2012).
[19]J. Zhang, J. Zhao, and J. Lu, ACS Nano **6**, 2704 (2012).
[20]Z. Song, V. I. Artyukhov, B. I. Yakobson, and Z. Xu, Nano Lett. **13**, 1829 (2013).
[21]J. Kotakoski and J. C. Meyer, Phys. Rev. B **85**, 195447 (2012).
[22]H. Zhang, Z. Duan, X. Zhang, C. Liu, J. Zhang, and J. Zhao, Phys. Chem. Chem. Phys. **15**, 11794 (2013).

[23]L. Yi, Z. Yin, Y. Zhang, and T. Chang, Carbon **51**, 373 (2013).
[24]Y. I. Jhon, S.-E. Zhu, J.-H. Ahn, and M. S. Jhon, Carbon **50**, 3708 (2012).
[25]M. Neek-Amal and F. M. Peeters, Appl. Phys. Lett. **100**, 101905 (2012).
[26]I. A. Ovid'ko and A. G. Sheinerman, J. Phys. D: Appl. Phys. **46**, 345305 (2013).
[27]S. S. Terdalkar, S. Huang, H. Yuan, J. J. Rencis, T. Zhu, and S. Zhang, Chem. Phys. Lett. **494**, 218 (2010).
[28]B. Zhang, G. Yang, and H. Xu, Physica B **434**, 145 (2014).
[29]K. Kim, V. I. Artyukhov, W. Regan, Y. Liu, M. F. Crommie, B. I. Yakobson, and A. Zettl, Nano Lett. **12**, 293 (2012).
[30]T. J. Booth, P. Blake, R. R. Nair, D. Jiang, E. W. Hill, U. Bangert, A. Bleloch, M. Gass, K. S. Novoselov, M. I. Katsnelson, and A. K. Geim, Nano Lett. **8**, 2442 (2008).
[31]S. Plimpton, J. Comput. Phys. **117**, 1 (1995).
[32]J. M. Carlsson, L. M. Ghiringhelli, and A. Fasolino, Phys. Rev. B **84**, 165423 (2011).
[33]J. Li, Modell. Simul. Mater. Sci. Eng. **11**, 173 (2003).
[34]G. Halsey, H. J. White, and H. Eyring, Textile Res. J. **15**, 295 (1945).
[35]C. Wei, K. Cho, and D. Srivastava, Phys. Rev. B **67**, 115407 (2003).
[36]H. Zhao and N. R. Aluru, J. Appl. Phys. **108**, 064321 (2010).
[37]J. Bailey, Glass Industry **20**, 95 (1939).
[38]D. W. Brenner, O. A. Shenderova, J. A. Harrison, S. J. Stuart, B. Ni, and S. B. Sinnott, J. Phys.: Condens. Matter **14**, 783 (2002).
[39]See supplementary material at http://dx.doi.org/10.1063/1.4883190 for results related to the energy barrier analysis of pristine graphene and a comparative energy barrier analysis of Σ 7 at T = 450 K.
[40]S. N. Zhurkov, Int. J. Fract. Mech. **1**, 311 (1965).
[41]J. C. M. Li, Surf. Sci. **31**, 12 (1972).